

Fe XVII X-ray lines in solar coronal and laboratory plasmas

K.J.H. Phillips¹, C.J. Greer², A.K. Bhatia³, I.H. Coffey², R. Barnsley⁴, and F.P. Keenan²

¹ Astrophysics Division, Rutherford Appleton Laboratory, Chilton, Didcot, Oxon. OX11 0QX, UK (phillips@solg2.bnsc.rl.ac.uk)

² Department of Physics, The Queen's University, Belfast BT7 1NN, Northern Ireland, UK

³ Laboratory for Astronomy and Solar Physics, NASA Goddard Space Flight Center, Greenbelt, MD 20771, USA

⁴ Department of Physics and Astronomy, Leicester University, Leicester LE1 7RH, UK

Received 27 September 1996 / Accepted 2 January 1997

Abstract. Theoretical intensities of the Fe XVII X-ray lines due to transitions $2p^6 - 2p^5 3d$ (near 15 Å) and $2p^6 - 2p^5 3s$ (near 17 Å) are presented, and compared with solar flare and active region spectra. The ratio of the 15 Å lines to the 17 Å lines is a function of temperature T_e , but for solar spectra this is not of practical use because of the resonance scattering of the intense 15.015 Å line. Instead we use the ratio of a nearby Fe XVIII line to obtain T_e . We find very satisfactory correspondence between solar spectra and synthetic spectra based on calculated line intensities with appropriately chosen T_e apart from the 15.015 Å line, which is sometimes less intense than its theoretical value, apparently owing to resonance scattering. Spectra emitted by DITE and JET tokamak plasmas with measured T_e and N_e are also considered. A predicted density variation of the ratio of the Fe XVII lines at 17.051 Å and 17.096 Å is confirmed, and using Abel inversion techniques applied to a sequence of DITE spectra with different radial distances good agreement is found between the theoretical temperature variation of the $I(15.015 \text{ Å})/I(16.776 \text{ Å})$ line ratio and that derived from these spectra. We conclude that our calculated Fe XVII line intensities are very reliable and may therefore be used in future analysis.

Key words: atomic data – atomic processes – Sun: activity – Sun: flares – Sun: X-rays, gamma rays

1. Introduction

The Fe XVII X-ray lines due to $2p^6 - 2p^5 3l$ ($l = s, d$) transitions have been extensively studied for many years. They occur in the wavelength region 15–17 Å in the spectra of solar active regions and flares, as well as plasmas produced in tokamaks and other laboratory devices, and can be expected to be present in the spectra of a wide variety of cosmic X-ray sources such as dMe stars and RS CVn binaries. The lines, which are the strongest of the solar X-ray spectrum with $\lambda < 20 \text{ Å}$, have peak emissivities at an electron temperature T_e of about 5 MK (1 MK = 10^6 K). They have some diagnostic potential, the ratio of the $2p^6 -$

$2p^5 3d$ lines (around 15 Å) and $2p^6 - 2p^5 3s$ (around 17 Å) lines being sensitive to T_e (Smith et al. 1985), though comparison with observed solar X-ray spectra (Rugge & McKenzie 1985; Schmelz, Saba, & Strong 1992; Waljeski et al. 1994; Phillips et al. 1996b) shows discrepancies which are due to resonance scattering of the most intense line at 15.015 Å. It has also been speculated, however, that inner-shell ionization of Na-like Fe (Fe^{+15}) ions significantly contributes to the excitation of the $2p^6 - 2p^5 3s$ lines (Feldman 1995). In addition, the ratio of two of the lines in the $2p^6 - 2p^5 3s$ array is a function of electron density for $N_e \gtrsim 10^{12} \text{ cm}^{-3}$.

Collision strengths using mostly the distorted wave procedure have been calculated by several authors (Loulergue & Nussbaumer 1975; Smith et al. 1985; Bhatia & Kastner 1985; Bhatia & Doschek 1992; Cornille, Dubau, & Jacquemot 1994; Cornille et al. 1994). The more recent of these calculations, which give collision strengths Ω at several energies rather than only one, can be expected to have greater reliability, since Ω appreciably varies with energy for some transitions. (We note that the R -matrix calculations of collision rates by Mohan (1993) are undoubtedly in error as they completely fail to reproduce observed solar or laboratory spectra, although the reasons for these discrepancies is not clear.)

Dielectronic satellites make a significant contribution to the spectrum. First, the stronger satellites may appear as discrete line features, and secondly, many weak satellites converging on Fe XVII lines may cumulatively be important and add to their intensities, so allowance must be made for them in calculating the temperature dependence of the 15 Å and 17 Å line ratios. Several of the above-cited works calculate satellite line intensities, as do Raymond & Smith (1986) and Nilsen (1989). As these satellites are mostly excited by dielectronic recombination, their intensities depend on T_e , so that the temperature derived from the relative intensities of the strongest discrete satellites could in principle be compared with that from the Fe XVII 15 Å and 17 Å line ratios.

Some Fe XVIII lines, with transitions $2s^2 2p^5 - 2s^2 2p^4 3s$ and $2s 2p^6 - 2s 2p^5 3s$, occur in the 15–17 Å region that includes the Fe XVII lines. Hence, provided the fractional abundances of

Send offprint requests to: K.J.H. Phillips

Fe⁺¹⁶ and Fe⁺¹⁷ ions can be obtained (e.g. from the steady-state coronal ionization equilibrium calculations of Arnaud & Raymond 1992, hereafter ARa), a further temperature diagnostic is available through the intensity ratio of Fe XVIII to Fe XVII lines. Application of all these temperature-dependent line intensities to solar spectra must assume that the emitting plasma either is isothermal, or has an assumed form for the distribution of emission measure with temperature.

In this paper, we use distorted wave calculations of Fe XVII collision strengths by Bhatia & Doschek (1992), together with calculated intensities of Fe XVI satellites and Fe XVIII lines in the same spectral region as the Fe XVII lines, to form synthetic spectra. These are subsequently compared with solar active region and flare spectra from the Flat Crystal Spectrometer on the *Solar Maximum Mission* (SMM) spacecraft. We also compare them with spectra emitted by high-temperature plasmas in the DITE and JET tokamak for which measured temperature and density profiles are available.

2. Atomic data

The Fe XVII lines at 15 Å are due to transitions between the ground state $2s^2 2p^6 1S_0$ and the $2s^2 2p^5 3d$ levels, while those at 17 Å are between the ground state and the $2s^2 2p^5 3s$ levels. The calculations of the atomic data, including the intensities of the X-ray lines, are described by Bhatia & Doschek (1992), where results are tabulated. We give a brief summary here.

The SUPERSTRUCTURE code (Eissner, Jones, & Nussbaumer 1974) was first run to obtain energy levels and radiative data in intermediate coupling. The configurations used were $2s^2 2p^6$, $2s^2 2p^5 3s$, $2s^2 2p^5 3p$, $2s^2 2p^5 3d$, $2s 2p^6 3s$, $2s 2p^6 3p$, and $2s 2p^6 3d$, representing 37 fine structure levels. A distorted-wave electron scattering program DSTWAV was then run, including intermediate states with L^T from 0 through 13 (L^T is the sum of the angular momenta of the incident electron and of the target level). Collision strengths Ω , calculated at five energies, were integrated over Maxwellian distributions to obtain excitation rate coefficients. Excitation by cascades from more highly excited configurations or by recombination of Fe⁺¹⁷ ions was neglected. Fractional level populations $n_j = N_j/N_T$ (N_j = number density of level j , N_T the sum of number densities of all levels), which were obtained by solving coupled rate equations, are tabulated by Bhatia & Doschek (1992) for various densities and two temperatures (4.0 and 7.3 MK), as are relative intensities ($A_{ji}n_j$ in units of photons s⁻¹) for the most intense lines.

In Table 1, we give relative intensities of the six most intense Fe XVII lines between 15 and 17 Å for $T_e = 2, 4, 6, 8,$ and 10 MK. The level labelling of Bhatia & Doschek (1992) is used, in particular, the $2p^5 3s^1 P_1$ and $^3 P_1$ levels are specified according to the *LS* designations of lower- Z Ne-like ions, i.e. the $^1 P_1$ level has the smaller energy of the two $J = 1$ levels, and so differs from that used by, e.g., Smith et al. (1985). According to ARa, Fe⁺¹⁶ ions represent at least 10% of the total number of Fe ions over this temperature range, as shown in Fig. 1 (a smaller fraction is indicated by Arnaud & Rothenflug [1985], also illustrated, which the ARa calculation updates). The intensities in Ta-

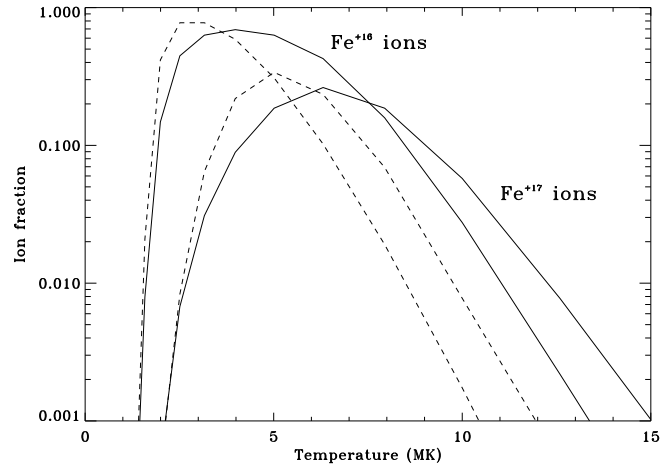


Fig. 1. Fe⁺¹⁶ and Fe⁺¹⁷ ion fractions as a function of T_e according to the coronal ionization equilibrium calculations of Arnaud & Rothenflug (1985) (dashed curves) and Arnaud & Raymond (1992) (solid curves).

ble 1 are given relative to the $2p^6 1S_0 - 2p^5 3s^3 P_1$ line (levels 1–5) for reasons discussed in Sect. 3, and for $N_e = 10^{10}$ cm⁻³ (the low-density limit for line intensity variations) and 10^{13} cm⁻³. We also give wavelengths of these lines from Bhatia & Doschek (1992), from Jupén & Litzén (1984) who used solar ultraviolet line wavelengths, and from observations with the Flat Crystal Spectrometer (FCS) on SMM of a flare on 1980 August 25 (Phillips et al. 1982). The SUPERSTRUCTURE wavelengths are between 0.02 Å and 0.04 Å smaller than those of Jupén & Litzén, which are close to the SMM values, apart from the $2p^6 1S_0 - 2p^5 3d^3 D_1$ line. Since Jupén & Litzén’s wavelength for this line appears to agree with that from most of the SMM spectra analyzed here, we adopt their wavelengths in the following.

The absolute photon flux (photons cm⁻² s⁻¹) of the 16.776 Å line (levels 1–5) emitted by a solar coronal plasma at the distance of the earth is given by

$$F_{1-5} = N_5 A_{5-1} V / 4\pi (\text{A.U.})^2 \quad (1)$$

where A_{5-1} is the transition rate, V the emitting volume (cm³), taken to be isothermal, and A.U. is an astronomical unit. With $n_5 = N_5/N_T$ and N_T practically equal to the total number density of all Fe⁺¹⁶ ions, Eq. (1) becomes

$$F_{1-5} = \frac{n_5 A_{5-1}}{N_e} \frac{N(\text{Fe}^{+16})}{N(\text{Fe})} B \quad (2)$$

where

$$B = \frac{N(\text{Fe})}{N(\text{H})} \frac{N(\text{H})}{N_e} \frac{N_e^2 V}{4\pi (\text{A.U.})^2}, \quad (3)$$

with $N(\text{Fe})/N(\text{H})$ the relative abundance of Fe to H, $N(\text{H})/N_e \approx 0.8$, and $N_e^2 V$ the isothermal emission measure.

An emissivity function $G(T_e)$ of the Fe XVII 16.776 Å line can be defined by

$$G(T_e) = \frac{n_5 A_{5-1}}{N_e} \frac{N(\text{Fe}^{+16})}{N(\text{Fe})} \frac{N(\text{Fe})}{N(\text{H})}. \quad (4)$$

Table 1. Chief Fe XVII lines used in the synthetic spectra. The wavelengths listed are respectively those calculated from the SUPERSTRUCTURE code (Bhatia & Doschek 1992) and by Jupén & Litzén (1984) and observed *SMM* values. The oscillator strengths (gf) are from Bhatia & Doschek (1992). Fluxes at the electron densities indicated are relative to the Fe XVII line at 16.776 Å (Jupén & Litzén’s wavelength).

Transition (including level labelling of Bhatia & Doschek 1992)	Jupén & Litzén Wavelength(Å)	SUPERSTRUCTURE Wavelength(Å)	<i>SMM</i> Wavelength(Å)	gf	$\log N_e$ (cm^{-3})	Calculated Intensity				
						T_e (MK)				
						2.0	4.0	6.0	8.0	10.0
$2p^6\ ^1S_0 - 2p^53s\ ^3P_2$ (1 - 2)	17.096	17.077	17.096	4×10^{-8}	10	1.064	0.922	0.856	0.822	0.801
					13	0.755	0.683	0.638	0.613	0.603
$2p^6\ ^1S_0 - 2p^53s\ ^1P_1$ (1 - 3)	17.051	17.031	17.051	0.123	10	1.204	1.182	1.172	1.171	1.169
					13	1.122	1.095	1.091	1.083	1.072
$2p^6\ ^1S_0 - 2p^53s\ ^3P_1$ (1 - 5)	16.776	16.759	16.775	0.101	10	1.000	1.000	1.000	1.000	1.000
					13	1.000	1.000	1.000	1.000	1.000
$2p^6\ ^1S_0 - 2p^53d\ ^3P_1$ (1 - 17)	15.450	15.432	15.451	0.009	10	0.120	0.101	0.090	0.085	0.082
					13	0.112	0.093	0.086	0.080	0.076
$2p^6\ ^1S_0 - 2p^53d\ ^3D_1$ (1 - 23)	15.262	15.234	15.255	0.593	10	0.538	0.616	0.660	0.712	0.798
					13	0.504	0.516	0.585	0.670	0.721
$2p^6\ ^1S_0 - 2p^53d\ ^1P_1$ (1 - 27)	15.015	14.972	15.012	2.662	10	1.089	1.358	1.677	2.217	3.254
					13	0.966	1.188	1.416	1.613	1.958

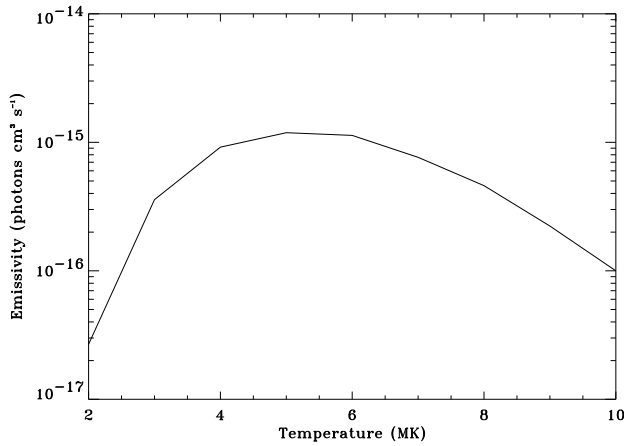


Fig. 2. Emissivity function $G(T_e)$, as defined in Eq. (4), for the Fe XVII 16.776 Å line.

Using the ARA ion fractions and $N(\text{Fe})/N(\text{H}) = 6.5 \times 10^{-5}$ (Feldman 1993), we calculated the $G(T_e)$ function as shown in Fig. 2. As can be seen, it peaks at a slightly greater temperature than the ionization fraction of Fe^{+16} ions.

We shall refer all measured and calculated line intensities to the 16.776 Å line, i.e. to the value F_{1-5}/B , so that the relative Fe abundance, the ionization fraction of Fe^{+16} ions, and the emission measure do not need to be specified for the construction of synthetic spectra (Sect. 3).

Fe XVI dielectronic satellites with transitions $2s^22p^6nl - 2s^22p^53s\ nl$ and $2s^22p^6nl - 2s^22p^53d\ nl$ occur near the Fe XVII 15.015 Å and 16.776 Å lines, respectively. Dielectronic recombination of the Fe^{+16} ion ($\text{Fe}^{+16}2p^6 + e \rightarrow \text{Fe}^{+15}2p^53l\ nl' \rightarrow$

$\text{Fe}^{+15}2p^6nl' + h\nu$) is the principal mechanism for exciting such satellites, the absolute photon fluxes of which are given by

$$F_{\text{diel}} = 2.07 \times 10^{-16} \frac{N(\text{Fe}^{+16})}{N(\text{Fe})} \frac{F_2 e^{-\Delta E/kT_e}}{T_e^{3/2}} B, \quad (5)$$

where ΔE is the energy of the satellite line’s upper level above the Fe XVII ground ($2p^6\ ^1S_0$) level and k is Boltzmann’s constant. The intensity factor F_2 is given by

$$F_2(j \rightarrow i) = \frac{g_j A_{ji}^r \sum_{m'} A_{jm'}^a}{\sum_{m'} A_{jm'}^a + \sum_{k'} A_{jk'}^r} \quad (6)$$

where the A^r are radiative transition rates between the levels stated, those in the summation being from level j to all possible levels k' below j , and the A^a are autoionization rates to all possible continua channels based on levels m' of the Ne-like ion lying below level j of the Na-like ion. These factors and wavelengths were derived from runs of the pseudo-relativistic Hartree–Fock (HFR) code of Cowan (1981). Arrays having ‘spectator’ or non-participating electrons with nl up to $5l$, $l = s, p$, and d were considered. Scaling factors of the Slater parameters, adjustments of which give small changes in the energy level intervals, were taken to be 100%, according to the prescription for high- Z ions by Cowan.

Values of F_{diel} for each satellite will be expressed relative to F_{1-5}/B (Eqs. (2) and (3)) in forming synthetic spectra, so that as before the relative Fe abundance, ionization fraction of Fe^{+16} ions, and emission measure are not specifically required.

Previous experience with the Cowan atomic code for calculations of Li-like satellites near He-like ion X-ray lines (Phillips et al., 1993, 1994; Harra-Murnion et al., 1996) has shown that a small, constant shift applied to the wavelengths from this code

Table 2. Comparison of calculated wavelengths and F_2 values (s^{-1}) for Fe XVI dielectronic satellites near the Fe XVII lines listed in Table 1. Satellites with $F_2 > 1.0(13)s^{-1}$ are included (numbers in parentheses are powers of 10 by which entries must be multiplied). Level notation is from the Cowan HFR code; alternative level designations from Cornille et al. (1994) are given in square brackets

Transition	Cowan/HFR Code		Cornille <i>et al.</i> (1994)	
	$\lambda(\text{\AA})$	F_2	$\lambda(\text{\AA})$	F_2
$2p^6 3d^2 D_{3/2} - 2p^5 3d^2 G_{5/2}$ [$^2F_{5/2}$]	15.496	1.40(13)	15.494	1.43(13)
$2p^6 3d^2 D_{5/2} - 2p^5 3d^2 G_{7/2}$	15.474	2.15(13)	15.473	1.74(13)
$2p^6 3d^2 D_{3/2} - 2p^5 3d^2 G_{5/2}$	15.464	1.07(13)	-	-
$2p^6 3d^2 D_{3/2} - 2p^5 3d^2 D_{1/2}$	15.407	1.05(13)	-	-
$2p^6 3d^2 D_{5/2} - 2p^5 3d^2 P_{3/2}$	15.376	1.04(13)	-	-
$2p^6 3d^2 D_{5/2} - 2p^5 3d^2 F_{7/2}$	15.353	2.06(13)	15.354	2.03(13)
$2p^6 3d^2 D_{3/2} - 2p^5 3d^2 F_{5/2}$	15.329	7.93(13)	15.321	8.77(13)
$2p^6 3p^2 P_{3/2} - 2p^5 3p3d^2 F_{5/2}$	15.264	5.48(13)	15.258	4.99(13)
$2p^6 3s^2 S_{1/2} - 2p^5 3s3d^2 P_{3/2}$	-	-	15.224	3.75(13)
$2p^6 3d^2 D_{3/2} - 2p^5 3d^2 P_{1/2}$	15.227	1.65(13)	15.205	1.96(13)
$2p^6 3d^2 D_{5/2} - 2p^5 3d^2 F_{7/2}$	15.205	1.05(14)	15.201	1.07(14)
$2p^6 3p^2 P_{1/2} - 2p^5 3p3d^2 D_{3/2}$	15.221	8.17(13)	15.201	8.10(13)
$2p^6 3p^2 P_{1/2} - 2p^5 3p3d^2 P_{1/2}$	15.212	1.77(13)	15.192	1.66(13)
$2p^6 3d^2 D_{5/2} - 2p^5 3d^2 D_{3/2}$	15.194	3.80(13)	15.174	3.33(13)
$2p^6 3s^2 S_{1/2} - 2p^5 3s3d^2 P_{1/2}$	15.181	1.54(13)	15.149	1.12(13)
$2p^6 3d^2 D_{5/2} - 2p^5 3d^2 D_{3/2}$	15.178	1.21(13)	-	-
$2p^6 3d^2 D_{3/2} - 2p^5 3d^2 D_{3/2}$	15.170	1.72(13)	15.146	1.22(13)
$2p^6 3p^2 P_{3/2} - 2p^5 3p3d^2 P_{1/2}$	15.173	2.54(13)	15.145	3.18(13)
$2p^6 3d^2 D_{5/2} - 2p^5 3d^2 P_{3/2}$	15.158	3.36(13)	15.135	4.14(13)
$2p^6 3d^2 D_{3/2} - 2p^5 3d^2 P_{3/2}$	15.150	3.56(13)	15.123	2.86(13)
$2p^6 3p^2 P_{3/2} - 2p^5 3p3d^2 P_{3/2}$ [$^2D_{3/2}$]	15.146	2.81(13)	15.111	2.35(13)
$2p^6 3p^2 P_{3/2} - 2p^5 3p3d^2 D_{5/2}$	15.138	2.97(13)	-	-
$2p^6 3s^2 S_{1/2} - 2p^5 3s3d^2 P_{3/2}$	15.148	2.37(13)	15.056	3.84(13)
$2p^6 3d^2 D_{3/2} - 2p^5 3d^2 P_{1/2}$	15.097	1.45(13)	15.040	1.24(13)
$2p^6 3p^2 P_{1/2} - 2p^5 3p3d^2 S_{1/2}$	15.069	1.40(13)	15.015	1.35(13)
$2p^6 3p^2 P_{3/2} - 2p^5 3p3d^2 D_{5/2}$	15.029	1.06(13)	-	-

brings them into approximate agreement with observed wavelengths, and that this shift can be found from comparison of the resonance line wavelengths and satellites with very high n values which should converge on to the resonance lines. A negligible shift ($0 \pm 0.02 \text{ \AA}$) was in fact found necessary for the Fe XVI satellites considered here by comparing $n = 9$ satellite wavelengths with those of the Fe XVII lines in Table 1.

The Fe XVI satellites calculated here have also been considered by Cornille et al. (1994). Table 2 gives the wavelengths and F_2 values for the 26 satellites with spectator electrons $3s$, $3p$, and $3d$ which have, according to our runs of the Cowan HFR code, values of F_2 larger than $10^{13} s^{-1}$. This list includes wavelengths and F_2 values given by Cornille et al. Where comparison is possible, the wavelengths from the two codes are in approximate agreement for lines with wavelengths longer than about 15.26 \AA . The Cowan wavelengths generally larger, however, by about 0.02 \AA , than those of Cornille et al. for most of the remainder. The F_2 values are mostly within 20% of each other, the best agreement being for those satellites with the largest values of F_2 . (The LS description of the upper level is sometimes ambiguous and the label given by the Cowan code is different from that given by Cornille et al. for two satellites; both alternatives are given.) Most of the line emission due to satellites with $3s$, $3p$, and $3d$ spectators according to the Cowan results occurs between 15.17 and 15.35 \AA , with several satellites blending with the Fe XVII 15.262 \AA line. Other satellites with $n = 4$

Table 3. Wavelengths and relative intensities of Fe XVI inner-shell satellites ($N_e = 10^8 \text{ cm}^{-3}$). The upper level of each transition is listed in column 1, the ground state being $2p^6 3s^2 S_{1/2}$ in each case. The notation is from the Cowan HFR code; alternative designations from the SUPERSTRUCTURE are given in square brackets. $\lambda_S =$ SUPERSTRUCTURE wavelength, $\lambda_C =$ wavelength from the Cowan HFR code.

Upper level of transition	$\lambda_S(\text{\AA})$	$\lambda_C(\text{\AA})$	Relative Intensity				
			$T_e(\text{MK}) =$				
			2	4	6	8	10
$2p^5 3s^2 P_{3/2}$	17.287	17.310	1.0	1.0	1.0	1.0	1.0
$2p^5 3s^2 P_{1/2}$	16.995	17.010	.24	.59	.65	.67	.68
$2p^5 3s3p^4 D_{5/2}$	16.697	16.721	.09	.16	.18	.18	.19
$2p^5 3s3p^4 D_{3/2}$	16.678	16.703	.03	.06	.07	.07	.07
$2p^5 3s3p^4 P_{5/2}$	16.610	16.634	.04	.13	.14	.15	.15
$2p^5 3s3p^2 D_{3/2}$ [$^4P_{3/2}$]	16.608	16.632	.02	.05	.06	.06	.06
$2p^5 3s3p^4 D_{3/2}$ [$^2P_{3/2}$]	16.406	16.424	.02	.04	.04	.04	.04
$2p^5 3s3d^4 P_{3/2}$	15.650	15.670	.02	.06	.07	.07	.08
$2p^5 3s3d^2 P_{1/2}$ [$^4D_{1/2}$]	15.543	15.563	.01	.04	.04	.04	.04
$2p^5 3s3d^2 P_{3/2}$ [$^4F_{3/2}$]	15.512	15.531	.04	.09	.11	.11	.11
$2p^5 3s3d^4 D_{1/2}$ [$^2P_{1/2}$]	15.433	15.451	.03	.09	.10	.11	.11
$2p^5 3s3d^4 D_{3/2}$ [$^2D_{3/2}$]	15.409	15.426	.01	.04	.04	.04	.05
$2p^5 3s3d^4 F_{3/2}$ [$^2D_{3/2}$]	15.354	15.369	.05	.15	.17	.17	.18
$2p^5 3s3d^2 D_{3/2}$ [$^2P_{3/2}$]	15.265	15.280	.08	.21	.24	.26	.26
$2p^5 3s3d^2 P_{1/2}$	15.162	15.181	.17	.47	.54	.57	.59
$2p^5 3s3d^2 P_{3/2}$	15.132	15.148	.27	.75	.86	.90	.93

and 5 spectators calculated with the Cowan code blend with the Fe XVII 15.015 \AA line.

Satellites in the $2p^6 3s - 2p^5 3s^2$, $2p^5 3s3p$, and $2p^5 3s3d$ arrays are also formed by inner-shell excitation from the ground level $2p^6 3s^2 S_{1/2}$ of Fe⁺¹⁵ ions. Inner-shell excitation from the $2p^6 3p$ and $2p^6 3d$ levels is insignificant as their populations are negligibly small for the low-density plasmas we consider. We calculated the intensities of inner-shell satellites $2p^6 3s - 2p^5 3s3l$ by running the SUPERSTRUCTURE and DSTWAV codes as with the Fe XVII line intensities. For this calculation, the 44 levels of the $2p^6 3s$, $2p^5 3s^2$, $2p^5 3s3p$, $2p^5 3s3d$ configurations were used. The calculations included intermediate states with L^T from 0 through 9. As inner-shell excitation of these satellites makes a relatively minor contribution to the X-ray spectrum, it was considered adequate to calculate collision strengths at only one energy, 62 Ry , and deriving rate coefficients by assuming the collision strengths to be constant with energy. In Table 3, we list the most intense of these satellites, with transitions, wavelengths (for consistency from the Cowan HFR code), transition rates, and intensities relative to the $2p^6 3s^2 S_{1/2} - 2p^5 3s^2 P_{3/2}$ line. As with the dielectronic satellites, there is often ambiguity in the labelling of the upper levels; the two alternatives are given in such cases. The Cowan code wavelengths are on average about 0.02 \AA larger than those from SUPERSTRUCTURE.

The absolute flux of Fe XVI satellites (e.g. that with transition 1–2) formed by inner-shell excitation is given by

$$F_{\text{is}} = \frac{n'_2 A'_{2-1}}{N_e} \frac{N(\text{Fe}^{+15})}{N(\text{Fe})} B \quad (7)$$

where n' and A' are analogous to the quantities in Eq. (2). This flux, when referred to the value of F_{1-5}/B in Eq. (2), thus requires Fe⁺¹⁵ ion fractions relative to Fe⁺¹⁶ which we obtained, in synthesizing spectra, from the ARa calculations.

Fe XVIII lines with transitions $2s^2 2p^5 - 2s^2 2p^4 3s$ occur between the Fe XVII 15 Å and 17 Å groups of lines. Calculated intensities using the SUPERSTRUCTURE and DSTWAV codes are available from Bhatia (1994) and Cornille et al. (1992) and using the R -matrix code from McKenzie et al. (1992). More detailed work with the R -matrix results may be found in Warren et al. (1997). These intensities, relative to the Fe XVII line intensities, allow temperature to be determined on the assumption of an isothermal emitting plasma. For consistency with the calculations being used for Fe XVII and Fe XVI inner-shell satellites, we used the work of Bhatia (1994).

The absolute flux of Fe XVIII lines, e.g. the strong line due to $2s^2 2p^5 \ ^2P_{3/2} - 2s^2 2p^4 \ (^3P) 3s^4 P_{5/2}$, with observed wavelength 16.073 Å, is given by

$$F_{\text{XVIII}} = \frac{n''_2 A''_{2-1}}{N_e} \frac{N(\text{Fe}^{+17})}{N(\text{Fe})} B \quad (8)$$

where n''_2 and A''_{2-1} are the fractional level population and transition rate by analogy with quantities in Eq. (2). As with Eq. (7), when F_{XVIII} is referred to F_{1-5}/B , Fe⁺¹⁷ ion fractions are required which were obtained from ARa. The intensities of three other lines in the $2s^2 2p^5 - 2s^2 2p^4 3s$ array relative to the 16.073 Å line are given in Table 4. There is (as was pointed out by McKenzie et al. 1992) little dependence of relative intensities on T_e so they are given for $T_e = 2$ and 10 MK only.

3. Synthetic spectra and diagnostic potential

Synthetic spectra were calculated from the intensities of all the lines mentioned above with a code used in previous work (Phillips et al. 1993). Each line was given a Voigt profile describing the main broadening mechanisms appropriate for the spectrometer viewing the spectrum. Thus for solar spectra viewed by the FCS instrument, these are the crystal rocking curve (approximately Lorentzian in shape) and thermal Doppler broadening (Gaussian). We assumed equal electron and ion temperatures (the equilibrium times defined by Spitzer [1962] are at most only a few seconds for expected flare densities and temperatures – see Phillips et al. 1996a). The instrumental broadening (0.012–0.015 Å FWHM over the 15–17 Å range) exceeds the thermal Doppler broadening by at least a factor of 2.5 over this temperature range. We neglected broadening due to the finite width of the FCS collimator (Sect. 4.1) which is between a third and a half of the thermal Doppler broadening. Both scanning-crystal and bent-crystal spectrometers were used for the DITE tokamak observations, and a scanning-crystal spectrometer for the JET observations. For the scanning spectrometers, the line

broadening is dominated by a slotted collimator, the FWHM being about 0.03 Å, which is larger than either the crystal rocking curve or the thermal Doppler broadening. The bent-crystal spectrometer has similar spectral resolution to the SMM FCS.

Fig. 3 shows synthetic spectra for six temperatures in the range 2 to 8 MK. These are calculated for the spectral resolution of the FCS instrument and for $N_e = 10^{10} \text{ cm}^{-3}$, i.e. in the low-density limit which is appropriate for the solar spectra considered here.

Unlike tokamak plasmas, for which there are usually independent means available for temperature and density determination, solar plasmas can only be diagnosed remotely, and the method recognized as being most direct is that using spectroscopic line intensity ratios. There are several lines in the 15–17 Å region which are possibly useful for the determination of temperature and density and we shall reconsider them here. We first discuss the meaning of a single value of temperature. The solar spectral data we shall compare the synthetic spectra with are from both non-flaring active regions and flares, mostly small ones of GOES class less than M1, though we also include two larger flares. For the times of the Fe XVII observations during the non-flaring active regions, we found from the spectral scans that there was no line present having an emissivity with higher temperature than the Mg XI line, which is marginally hotter than the Fe XVII 16.776 Å line. If the temperature dependence of the differential emission measure is like that found for active regions by Brosius et al. (1996) from SERTS extreme ultraviolet data, having a peak in the distribution at $\log T_e = 6.0$ –6.6, we could reasonably deduce that the X-ray plasma is approximately isothermal, with temperature given by the Fe XVII spectra. For the flares, particularly those with GOES class greater than about C3, there is emission in much hotter ions, e.g. He-like Ca ($T_e \gtrsim 14$ MK) which has lines in the spectral region viewed by the SMM Bent Crystal Spectrometer (BCS). Thus, these plasmas are clearly non-isothermal, and the temperature deduced from the Fe XVII spectra is an average of the cooler portion of the flare plasma.

Both the JET and DITE tokamak plasmas have central temperatures that are higher than the temperature of maximum $G(T_e)$ of the Fe XVII lines (Fig. 2), so the Fe XVII line emission arises from a shell around the central part of the plasma. When observed by a spectrometer along a central chord, the resulting spectrum therefore has a characteristic temperature $T_e \approx 6$ MK but with contributions to the emission from regions inside and outside of this shell, where the plasma is respectively hotter and cooler than this value.

It can be seen from Fig. 3 that the intensity ratio of the three Fe XVII $2p^6 - 2p^5 3d$ lines near 15 Å to the three Fe XVII $2p^6 - 2p^5 3s$ lines near 17 Å varies appreciably with temperature, the 3d lines becoming relatively more intense with increasing temperature. This potential temperature diagnostic was pointed out by Rugge & McKenzie (1985), Raymond & Smith (1986), and Cornille et al. (1994). The theoretical temperature dependence of these lines can be more clearly seen from Fig. 4, the solid curves of which show the peak intensity of each Fe XVII line feature measured from the synthetic spectra of Fig. 3 rel-

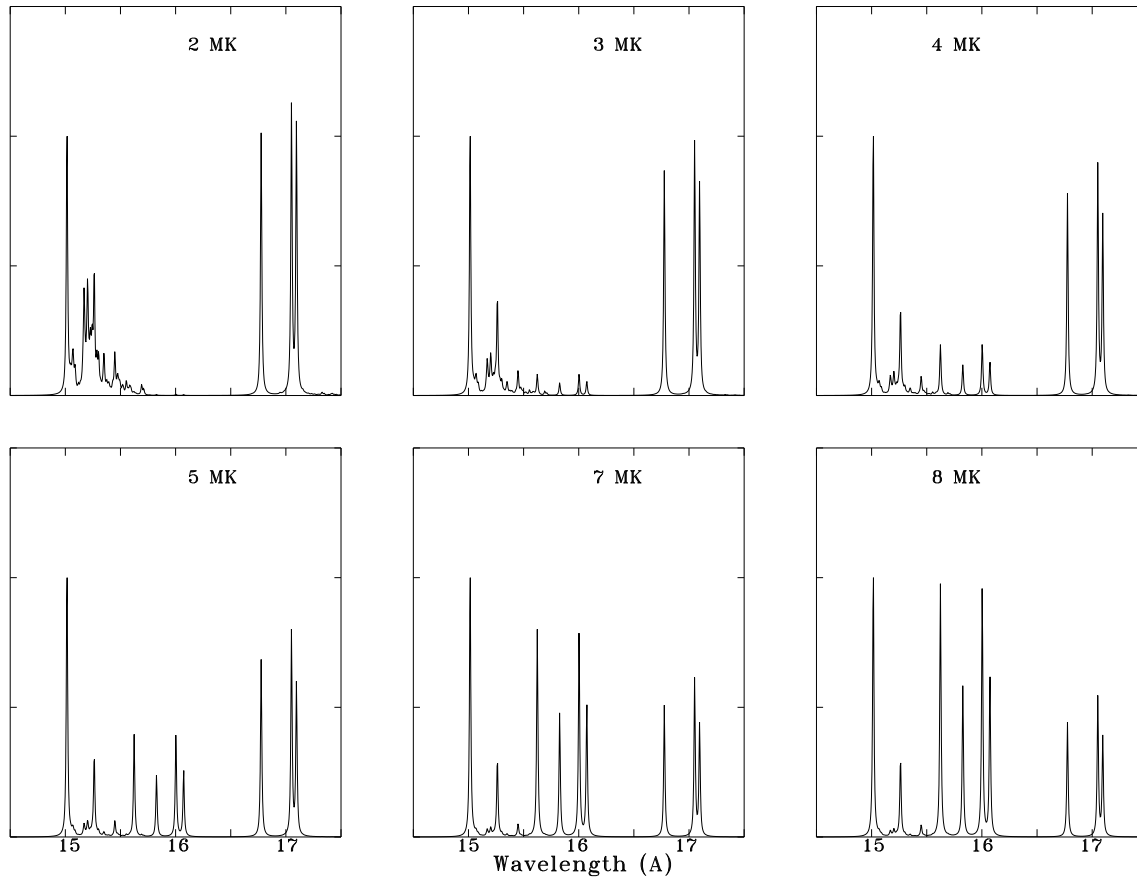


Fig. 3. Synthetic spectra showing Fe XVII lines together with Fe XVI dielectronic satellites and four of the Fe XVIII lines in the $2p^5 - 2p^4 3s$ array. Plots are for the temperatures indicated and for an electron density equal to 10^{11} cm^{-3} , the low-density limit.

ative to the peak intensity of the 16.776 Å resonance line as a function of T_e in the low-density limit. As peak intensities are plotted, the effects of unresolved Fe XVI satellites are included. The dashed curves show the Fe XVII line ratios without the satellite contribution, and are essentially the low-density-limit values shown in Table 1. As expected, the greatest divergence between the solid and dashed curves is at low temperatures when the relative contribution of the Fe XVI satellites is greatest. In previous work the Fe XVII 15.015 Å line was chosen as a reference, but because of the possibly large effect of resonance scattering on this line we have expressed intensities in Fig. 4 in terms of the 16.776 Å line.

The practical use of these ratios as temperature diagnostics is more limited than has been previously suggested, owing principally to the fact that the intensity of the most important of the $2p^6 - 2p^5 3d$ lines, that at 15.015 Å, is subject to unknown variations because of the effect of resonance scattering. Discarding this line then leaves only the weaker line at 15.262 Å and the much weaker line at 15.450 Å in this array. Of the three $2p^6 - 2p^5 3s$ lines, the variation with N_e of the 17.096 Å line for $N_e \gtrsim 10^{12} \text{ cm}^{-3}$ (see below) makes this line undesirable as a temperature diagnostic for tokamak plasmas. Thus, the ratio of the 15.262 Å line to the 16.776 Å line is in effect the only

one available for measuring T_e in solar spectra and even this is problematical. Apart from the weakness of the 15.262 Å line, the dependence of the $I(15.262 \text{ Å})/I(16.776 \text{ Å})$ intensity ratio on T_e , because of the contribution of blended Fe XVI satellites, is not single-valued for $T_e \lesssim 3 \text{ MK}$ and only has a relatively strong T_e dependence for $T_e > 6 \text{ MK}$, higher than the temperatures describing the solar spectra considered here.

Fe XVI satellites were considered by Raymond & Smith (1986), who found that the contribution made by all those in the $2p^5 3d nl - 2p^6 3d$ array falling near the 15 Å Fe XVII lines was very significant (e.g. more than 60% of the total intensity at $T_e = 2.5 \text{ MK}$). Raymond & Smith also considered the temperature diagnostic potential of the ratio of discrete Fe XVI satellites to the Fe XVII 15.015 Å line. In principle, this should be useful as with Li-like dielectronic satellites near He-like ion resonance lines (Gabriel 1972). However, we point out two factors that render this diagnostic impractical for use with solar spectra. The first is the wavelength accuracy of present satellite calculations which, as Table 2 indicates, is probably not better than about 0.02 Å. If random uncertainties of 0.01 Å are admitted, it is unlikely that the pattern of satellite line emission in synthetic spectra between, say, 15.0 and 15.5 Å, can be calculated for a sufficiently certain comparison with observed emission.

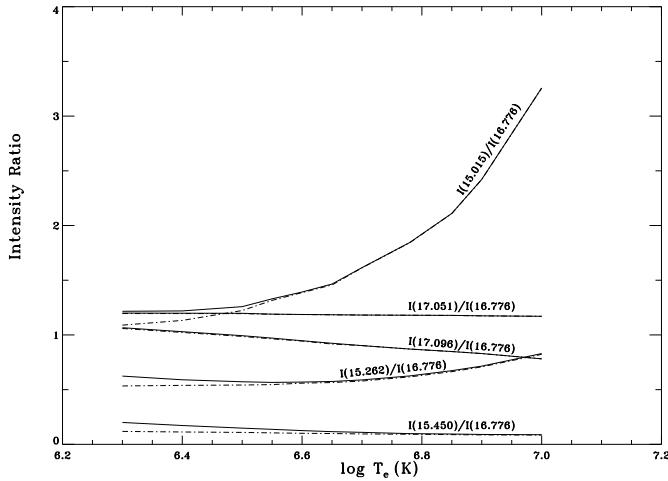


Fig. 4. Ratios of peak intensities, measured from synthetic spectra, of the Fe XVII lines listed in Table 1 and indicated in the labels plotted against T_e . Ratios calculated in low-density limit. Solid curves show theoretical ratios including the contributions of Fe XVI satellites, dot-dash curves, excluding them.

The second is the occurrence of the O VIII Ly γ ($1s - 4p$) line at 15.176 Å (Erickson 1977) and an Fe XIX line at around 15.17 Å in the $2p^4 - 2p^3 3s$ array (Phillips et al. 1982). The uncertainty in the wavelength of the latter line particularly makes it virtually impossible to unravel the contribution to the observed emission made by Fe XVI satellites in the vicinity of 15.18 Å, so rendering them unusable. Some Fe XVI satellite emission around 15.07 Å is barely distinguishable from the Fe XVII 15.015 Å line, but such emission is too weak to be an accurate temperature diagnostic.

In summary, the temperature-dependent line ratios involving either Fe XVII lines or Fe XVI dielectronic satellites do not appear to have much practical application for solar spectra.

As already indicated, a possible third temperature diagnostic is provided by nearby Fe XVIII lines. Previous work has used the ratio of the strong Fe XVIII $2p^5 2P_{3/2} - 2p^4 3d^2 D_{5/2}$ line at 14.204 Å to the Fe XVII 15.015 Å line (Rugge & McKenzie 1985, Saba & Strong 1992). For the purposes of this work, we use an intensity ratio (denoted by R_1) of the strong Fe XVIII line at 16.073 Å (due to $2p^5 2P_{3/2} - 2p^4 ({}^3P) 3s^4 P_{5/2}$: see Table 4) to the Fe XVII 16.776 Å line. This Fe XVIII line is included in all the FCS spectra discussed here. It is unblended, though the O VIII Ly β ($1s - 3p$) line falls nearby, at 16.006 Å. Fig. 5 shows the temperature dependence of the R_1 ratio as calculated from Eqs. (2) and (8), using the ARa ionization fractions. As can be seen, R_1 strongly depends on T_e and we will use it here to determine T_e .

The Fe XVII line ratio $I(17.096 \text{ \AA})/I(17.051 \text{ \AA})$ (denoted by R_2) decreases with N_e for $N_e \gtrsim 10^{12} \text{ cm}^{-3}$, a fact pointed out for iso-electronic ions with smaller Z by Bhatia & Kastner (1985). The reason is that at high densities collisional de-excitation competes with spontaneous de-excitation from the $2p^5 3s^3 P_2$ state to the ground state. Fig. 6 shows the R_2 inten-

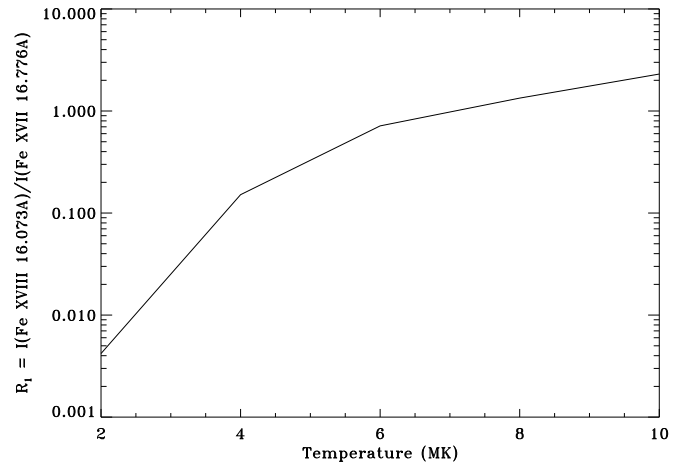


Fig. 5. Temperature dependence of the R_1 ratio of the Fe XVIII line at 16.073 Å line to the Fe XVII line at 16.776 Å, calculated in the low-density limit.

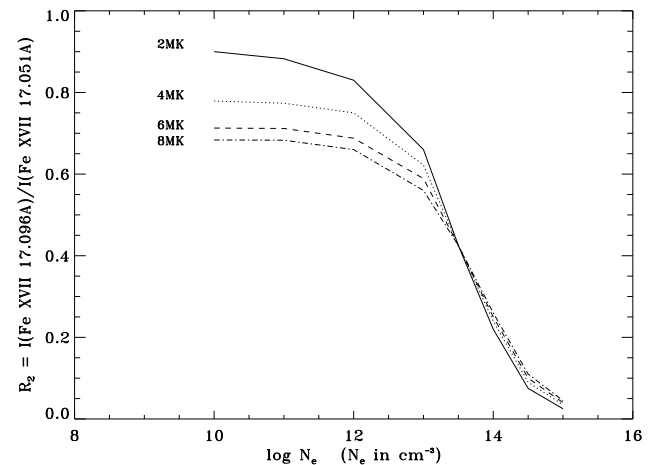


Fig. 6. The peak intensity ratio R_2 of the Fe XVII line at 17.096 Å to that at 17.051 Å plotted against N_e for the temperatures indicated.

sity ratio measured from the synthetic spectra plotted against N_e for the temperatures indicated. This ratio is thus useful as a density diagnostic for plasmas having $N_e \gtrsim 10^{12} \text{ cm}^{-3}$, i.e. those appropriate to tokamak plasmas but not solar active regions or flares in their decay phase.

4. Observed spectra and comparison with theory

4.1. Solar active region and flare spectra

The FCS instrument on *SMM* and analysis of the data have been described in detail elsewhere (Acton et al. 1980, Phillips et al. 1982). Spectra were generally observed by aiming the FCS at the brightest part of an emitting region, in a predetermined sequence, and then performing wavelength scans over specific ranges in steps of one or more units of $9.9''$, with dwell times of typically 1 second or less at each spectral location. Both the relative and absolute wavelength accuracy of the FCS is

Table 4. Fe XVIII lines used in the analysis. Wavelengths and relative intensities (10^{10} cm^{-3}) are from Bhatia (1994). Level notation is from this paper, with alternative designations from Cornille et al. (1992)

Transition	$\lambda(\text{\AA})$	Relative Intensity	
		$T_e =$	
		2MK	10MK
$2p^5 \ ^2P_{3/2} - 2p^4(^3P)3s \ ^4P_{3/2}$	16.073	1.00	1.00
$2p^5 \ ^2P_{3/2} - 2p^4(^3P)3s \ ^4P_{3/2} \ [^2P_{3/2}]$	16.003	1.44	1.58
$2p^5 \ ^2P_{3/2} - 2p^4(^3P)3s \ ^2P_{3/2} \ [^4P_{3/2}]$	15.827	0.85	0.95
$2p^5 \ ^2P_{3/2} - 2p^4(^1D)3s \ ^2D_{5/2}$	15.624	1.38	1.58

extremely high, of order 0.001 \AA or less for the KAP crystal channel (Phillips et al. 1982). The sensitivity of the FCS was determined from prelaunch measurements and calculations, and factors expressing the sensitivity as a function of wavelength can be applied to raw spectral data to give absolute units using interactive computer programs.

Spectra covering the 15–17 \AA wavelength range were recorded by the FCS on many occasions over the spacecraft lifetime (1980–1989), most of them from nonflaring active regions and small flares. A significant problem in flare spectra is the time variation of emission that often occurred while scanning spectra. For example, a typical scan time between 15 \AA and 17 \AA was 3 minutes, so that for spectra recorded by the FCS scanning this range during a flare decay in the direction of increasing wavelength, the intensities of the Fe XVII 17 \AA lines would be smaller than expected compared with the 15 \AA lines. We tried to overcome this problem by selecting spectra for which the X-ray emission in the region of the He-like calcium (Ca XIX) resonance line at 3.17 \AA , recorded by the companion Bent Crystal Spectrometer (BCS), was reasonably constant during the FCS scan time.

Table 5 lists spectra that were selected for detailed analysis. For the flare spectra, the *GOES* X-ray classification is listed. Observed line fluxes are given for the Fe XVII lines of Table 1 relative to the 16.776 \AA line, obtained by best-fit Voigt profiles to the observed line spectra, using standard software based on a gradient search of the location of least χ^2 in parameter space. The temperature estimated from the R_1 ratio defined above is also listed.

The observed line ratios are subject to statistical uncertainties in count rates. For the more intense flare spectra, with integrated count rates of more than 1000 s^{-1} , we estimate the uncertainties in the ratios to be only 4% or smaller. For the active region spectra, with count rates up to about a factor 20 less than for flares, we estimate the uncertainties to be up to 8%, or about 15% for the weak 15.450 \AA line, and about 14% for the Fe XVIII line at 16.073 \AA , used for estimating temperature. Systematic uncertainties are possible arising from the calculation of the spectrometer's relative sensitivity over the spectral range 15–17 \AA (Acton et al. 1980), but these are likely to be less than 2%. The corresponding uncertainties ΔT_e in estimated temperatures are $\Delta T_e \approx 0.1 \text{ MK}$ for flare spectra, $\approx 0.25 \text{ MK}$ for active region spectra.

Fig. 7 shows some of these observations with synthetic spectra in the low-density limit overlaid with temperatures equal to that from the R_1 ratio. The spectral flux is expressed in absolute units (photons s^{-1} per wavelength interval of 0.0010 \AA), and the observed and synthetic spectra are normalized to the 16.776 \AA line peak. The background in each spectrum is mostly instrumental. Spectra (a) and (b) are from nonflaring active regions, (c) and (d) from flares. There is generally very close agreement between the observed and synthetic spectra for the Fe XVII lines at 15.262, 15.450, 17.051, and 17.096 \AA , even for flare spectra when small intensity variations over the scan times might be expected. The observed flux of the 15.015 \AA line, however, is less than the calculated by a factor that varies between 0.24 and nearly 1. The Fe XVIII lines also show some disagreement. Thus, the observed 16.003 \AA line is sometimes less, other times more, intense than the calculated, despite the fact one would expect, with the presence of the O VIII line at 16.006 \AA , that the observed would generally be more intense than the calculated.

The agreement of the Fe XVII observed and calculated line fluxes is dramatically illustrated in Figs. 8a–e, in which the calculated curves of Fig. 4 and observed points are placed on each plot against T_e . Uncertainties in the ratios as estimated above are shown as error bars. As can be seen, there is agreement with the theoretical curves of Fig. 4 to within the estimated uncertainties for the ratios $I(15.450 \text{ \AA})/I(16.776 \text{ \AA})$, $I(17.051 \text{ \AA})/I(16.776 \text{ \AA})$, and $I(17.096 \text{ \AA})/I(16.776 \text{ \AA})$, in particular the observed points following the theoretical variation with T_e . This can be regarded as a confirmation of the accuracy of the distorted wave calculations of the Fe XVII collision strengths for the appropriate transitions. With the $I(15.262 \text{ \AA})/I(16.776 \text{ \AA})$ ratio, the observed points tend to be below the theory curve, and with the $I(15.015 \text{ \AA})/I(16.776 \text{ \AA})$ ratio the points are considerably below. The spread of points is much larger than the estimated uncertainties, especially for the 15.015 \AA line. The reason appears to be associated with resonance scattering in each case, the oscillator strengths of each line being large (see Table 1). As discussed by Phillips et al. (1996b), the reason is that the emitting region, either flare or central part of the active region, is denser than the surrounding material, and photons are therefore scattered out of the line of sight. The disagreement between theoretical and observed line fluxes for these two cases can be easily explained, and is not therefore an indication of the accuracy of the atomic calculations.

4.2. Tokamak spectra

Fe XVII line emission has been observed from the plasmas of several laboratory devices. Here we discuss spectra from the Divertor-Injector Tokamak Experiment (DITE), which was used as an experimental device at the Culham Laboratory, UK, and the Joint European Torus (JET), used for thermonuclear fusion research. They have been described by Allen et al. (1986) and Rebut et al. (1987). The major and minor radii of the DITE device were 1.7 m and 24 cm respectively, the toroidal field 2.4 T and plasma current 150 kA. The central region of the plasma

Table 5. Observed flare and active region Fe XVII line fluxes. Times refer to start of FCS scans. The positions are heliographic coordinates of the FCS pointing, with active region (AR) identified from the NOAA *Solar Geophysical Data Bulletin*. Line fluxes (normalized to the 16.776 Å line) are integrated over profiles.

a) Active Regions

Date	UT of FCS Scan	Position	AR	T_e (MK)	Observed Fe XVII line fluxes relative to 16.776 Å line				
					15.015 Å	15.262 Å	15.450 Å	17.051 Å	17.096 Å
14-Feb-86	04:29	S20W85	4713	3.7	1.15	0.43	0.07	1.13	1.00
...	04:43	3.4	1.25	0.46	0.07	1.16	0.90
18-May-86	20:07	N05E90	4731	3.5	1.18	0.42	0.07	1.15	1.01
...	20:16	3.3	1.22	0.42	0.08	1.14	0.90
...	20:26	2.9	1.18	0.51	0.08	1.15	1.03
21-May-86	14:16	N07E50	4731	3.2	0.82	0.44	0.07	1.14	1.03
...	14:26	3.8	0.79	0.40	0.06	1.14	1.00
...	14:35	3.5	0.81	0.46	0.07	1.09	1.04
24-May-86	05:03	N08E12	4731	3.3	0.46	0.51	0.07	1.12	1.02
...	05:13	3.8	0.66	0.42	0.08	1.15	0.98
...	05:22	3.5	0.72	0.44	0.07	1.10	1.02
13-Jul-86	04:31	N08W79	4736	3.3	1.07	0.46	0.08	1.13	1.01
14-Jul-86	15:20	N08W90	4736	4.1	1.25	0.45	0.07	1.09	0.93
09-Apr-87	21:50	S35E45	4787	4.2	0.87	0.45	0.07	1.08	0.89
...	22:00	3.9	0.82	0.49	0.07	1.13	1.01
...	22:09	4.5	0.82	0.46	0.07	1.14	1.00
...	22:19	5.0	0.84	0.48	0.07	1.14	1.01
13-Apr-87	01:14	S34W02	...	4.1	0.70	0.47	0.07	1.15	0.94
...	01:24	3.8	0.77	0.45	0.07	1.09	1.03
...	01:33	4.1	0.62	0.43	0.07	1.15	0.94
...	01:43	4.0	0.72	0.33	0.07	1.09	0.92
15-Apr-87	16:04	S35W36	4787	3.8	0.88	0.46	0.08	1.12	1.02
...	16:13	4.5	0.85	0.49	0.07	1.15	0.88
...	22:34	S35W40	...	3.3	0.75	0.45	0.07	1.03	1.02
...	23:55	4.0	0.82	0.49	0.07	1.13	0.91
16-Apr-87	00:05	S35W41	...	4.3	0.99	0.54	0.08	1.19	0.86
...	08:11	S33W45	...	4.1	0.86	0.46	0.08	1.18	1.00
...	17:42	S35W53	...	4.8	1.01	0.50	0.07	1.16	0.83
...	18:47	4.3	0.78	0.44	0.07	1.13	1.01
17-Apr-87	03:07	S35W58	...	4.8	0.85	0.46	0.07	1.05	1.03
...	20:24	S35W70	...	4.0	1.18	0.45	0.08	1.13	0.93
18-Apr-87	05:38	S33W75	...	4.0	1.10	0.50	0.07	1.14	1.02
...	05:52	3.8	1.09	0.49	0.07	1.12	0.95
...	22:37	S33W85	...	4.6	1.41	0.47	0.09	1.06	0.83
19-Apr-87	14:41	S35W90	...	3.7	1.50	0.50	0.08	1.15	0.80
...	14:56	3.7	1.27	0.46	0.07	1.31	0.92
...	16:23	S35W90	...	3.8	1.20	0.51	0.07	1.07	0.98
...	16:32	3.7	1.29	0.49	0.07	1.17	0.92
22-May-87	20:50	N30W02	4811	4.1	0.71	0.44	0.08	1.23	0.89
27-Nov-87	16:25	S22W65	4891	2.9	1.09	0.37	0.07	1.15	1.00
...	16:35	3.3	1.09	0.42	0.07	1.12	0.98
...	16:45	3.1	1.09	0.41	0.07	1.11	1.03
...	16:54	3.0	1.13	0.39	0.06	1.10	1.02

was characterized by $T_e \approx 8.7 \pm 0.9$ MK (750 ± 75 eV) and $N_e \approx 3 \times 10^{13}$ cm $^{-3}$. The major and minor radii of the JET device are 2.96 m and 1.25 m respectively, and the maximum toroidal field is 3.45 T, the maximum toroidal current 7 MA. A variety of heating mechanisms have been applied to JET plasmas over the past few years, with electron temperatures up to 140 MK (12 keV) and densities up to 2×10^{14} cm $^{-3}$ having been achieved. The measurements described here were taken with the plasma ohmically heated (i.e. not additionally heated), with central temperature 2.5 keV and density 3.2×10^{13} cm $^{-3}$.

Several Fe XVII spectra were obtained with the DITE device in 1984. Fig. 9 shows a spectrum between 16.6 Å and 17.3 Å (dotted line) observed through a central chord of the plasma by a spectrometer with Johann geometry, having a curved KAP crystal ($2d = 26.62$ Å) and position-sensitive channel plate detector with delay line readout (see Duval et al. 1986 for further details). Corrections for the slight variation of instrument sensitivity over the spectral range shown have been applied. The spectrum was integrated during a steady-state period of the discharge, with line-integral of electron density equal to 2×10^{13} cm $^{-3}$. The resolution of the spectrometer is comparable to that of the FCS,

Table 5. (continued)

Date	UT of FCS Scan	GOES class	Position	AR	T_e (MK)	Observed Fe XVII line fluxes relative to 16.776 Å line				
						15.015 Å	15.262 Å	15.450 Å	17.051 Å	17.096 Å
19-Oct-86	01:49	M5	N20E61	4750	5.4	1.36	0.57	0.09	1.17	0.87
...	02:04	5.5	1.04	0.45	0.07	1.15	0.90
...	02:18	5.0	1.09	0.47	0.08	1.10	0.91
...	02:32	4.7	1.10	0.46	0.07	1.17	0.87
...	03:24	5.3	1.08	0.44	0.07	1.14	0.90
...	03:38	...	N20E62	...	4.7	0.99	0.43	0.07	1.07	1.00
...	04:58	5.1	0.88	0.38	0.07	1.14	0.89
...	05:12	4.8	0.93	0.43	0.08	1.14	0.91
25-Aug-80	13:10	M1	N20W56	2629	4.9	1.00	0.47	0.08	1.15	0.86
26-May-87	20:09	C8	N45W70	4811	5.7	1.21	0.49	0.08	1.16	0.87
...	20:24	4.8	1.18	0.44	0.07	1.16	0.89
13-Feb-86	05:08	C7	N05W64	4713	4.7	1.08	0.45	0.07	1.16	0.87
16-Apr-87	17:27	C7	S35W55	4787	4.5	0.84	0.45	0.07	1.14	1.01
03-Mar-86	14:43	C5	N02E50	4717	5.1	0.88	0.47	0.07	1.14	0.90
...	14:52	4.8	0.83	0.50	0.07	1.12	0.85
...	15:02	4.8	0.85	0.46	0.07	1.13	0.96
10-Jul-86	18:07	C4	N05W48	4736	4.5	0.85	0.44	0.07	1.12	1.00
17-Oct-86	05:51	C4	N23E90	4750	5.1	1.40	0.46	0.07	1.15	0.83
...	06:05	4.8	1.36	0.45	0.08	1.15	0.90
...	06:19	4.3	1.18	0.45	0.07	1.14	0.92
11-Jul-86	05:24	C3	N08W55	4736	4.5	0.79	0.52	0.07	1.14	0.97
07-Mar-86	00:08	C2	S00W02	4717	5.3	0.68	0.49	0.08	1.16	0.85
13-Jul-86	01:08	C2	N08W78	4736	3.5	0.97	0.39	0.07	1.08	1.00
...	01:22	3.8	1.12	0.45	0.07	1.14	1.01
...	01:37	4.1	1.25	0.52	0.07	1.14	0.92
...	02:42	...	N08W79	...	4.7	1.25	0.49	0.10	1.16	0.79
...	02:57	4.3	1.27	0.47	0.08	1.15	0.99
...	03:11	3.9	1.31	0.51	0.08	1.12	1.00
17-Apr-87	17:26	C2	S23W75	4787	5.1	1.33	0.48	0.06	1.20	0.79
21-May-87	19:28	C2	N30E10	4811	3.6	0.90	0.47	0.08	1.20	1.00
...	19:42	3.7	0.66	0.44	0.07	1.06	1.01
18-Apr-87	22:56	C1	S33W90	4787	4.3	1.34	0.39	0.07	1.15	0.93
...	23:06	4.0	1.41	0.50	0.08	1.14	0.80
22-May-87	20:21	B8	N30W02	4811	4.8	0.80	0.46	0.07	1.17	0.89

Note: GOES class refers to peak of flare.

and so we have used Voigt profiles with the definitions used above. The solid curve shows the best fit to the observed spectrum with $T_e = 9$ MK and $N_e = 1 \times 10^{13}$ cm $^{-3}$, normalizing to the Fe XVII 16.776 Å line. It illustrates how good the fit is to the pair of Fe XVII lines at 17.051 Å and 17.096 Å, and confirms the variation with N_e shown in Fig. 6.

Fig. 10 shows one of a sequence of longer-scan spectra from the DITE tokamak taken in 1987, each obtained with a Bragg rotor spectrometer with RAP crystal ($2d = 26.12$ Å) which rotates continuously during a plasma shot (see Barnsley 1986 for details). The spectral resolution (see Sect. 3) is essentially determined by a slotted collimator, the line profiles having FWHM equal to 0.03 Å at around 16 Å. The spectrum is corrected for variations in instrumental sensitivity over this range. Spectra in the sequence were formed along chords having various distances from the plasma centre, the spectrum of Fig. 10 being the central-chord spectrum. The central temperature ($T_e = 8.7$ MK) was measured by Thomson scattering, and the line-integrated

electron density (2.1×10^{13} cm $^{-3}$) by microwave interferometry (the peak density is $1.5 \times$ this value). In the absence of profile measurements for these specific discharges, we assumed functional forms for the radial variation of temperature and density, based on measurements for other discharges. For temperature, we assumed

$$T_e(r) = T(0)(1 - r^2/a^2)^2, \quad (9)$$

and of density,

$$N_e(r) = N_e(0)(1 - r^2/a^2), \quad (10)$$

where r is the radial variable and a the minor radius of the DITE plasma, being 24 cm. Normally, the functional forms should involve the temperature and density of the outer regions of the plasma, but these were found to have only a small effect for our purposes.

With this sequence of spectra, we were able to use Abel inversion techniques to obtain the radial variation of line emissivities, in particular those of the Fe XVII 15.015 Å and 16.776 Å

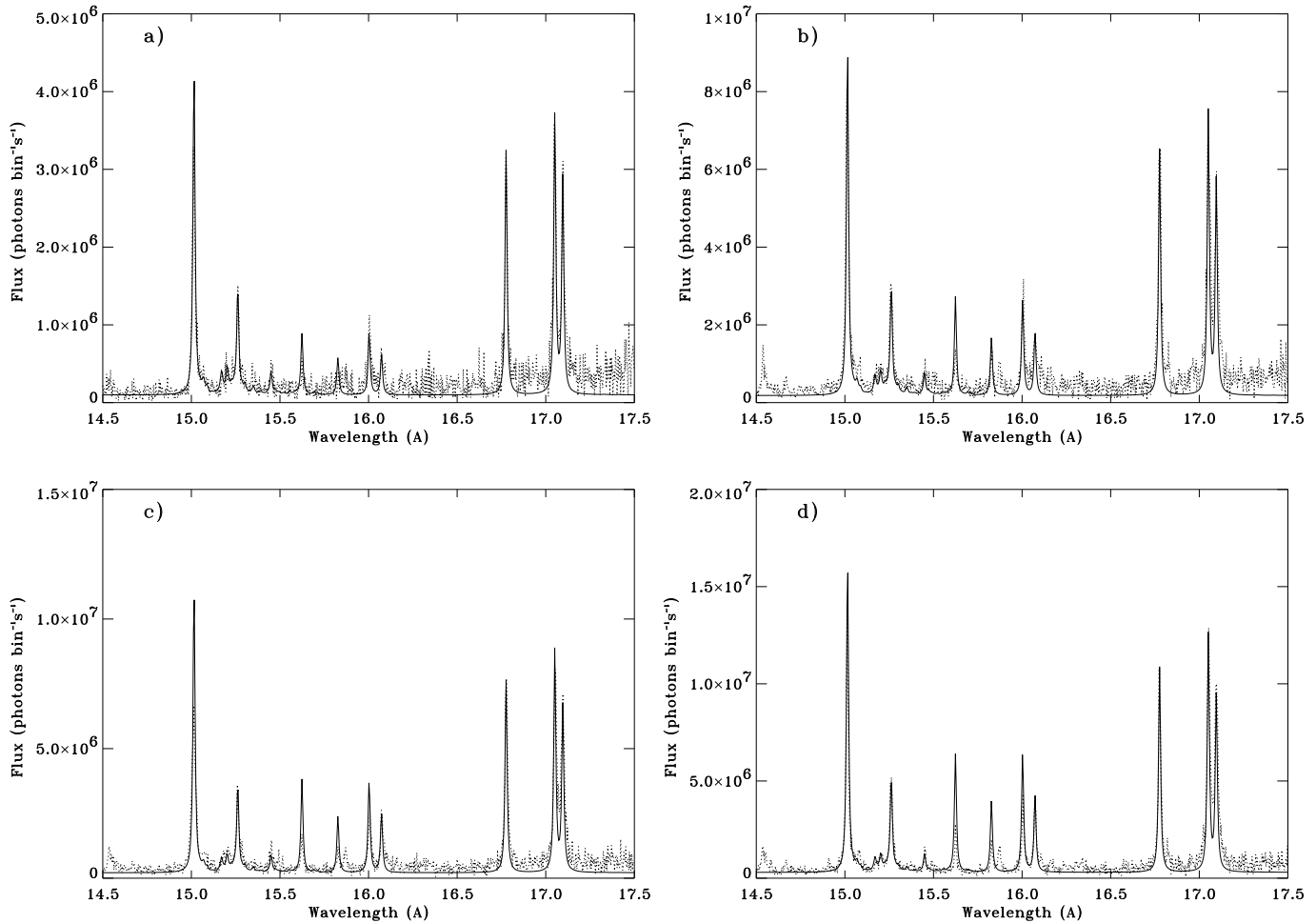


Fig. 7a–d. Four observed spectra in the region of the Fe XVII lines (dotted curve) compared with synthetic spectra (solid lines) calculated in the low-density limit at temperatures T_e found from the R_1 ratio. Times of the spectra are: **a** 1987 April 9 (2200:11 UT); **b** 1987 April 18 (2237:14 UT); **c** 1986 March 3 (1452:43 UT); **d** 1986 October 17 (0551:05 UT). Spectra **a** and **b** are from nonflaring active regions, spectra **c** and **d** from small flares (see Table 5).

lines. Fig. 11 shows these emissivities E as a function of r , together with their ratio $E(15.015)/E(16.776)$, and illustrates how the Fe XVII line emission in the DITE plasma originates in a shell with $r = 9$ cm, or $r/a \approx 0.4$. The observed spectrum in Fig. 10 is therefore compared with a theoretical one (solid line) having values of N_e and T_e appropriate to this shell. Since the Fe XVIII line emission originates in a shell nearer the plasma centre where T_e is higher, we omit Fe XVIII lines from the theoretical spectrum, which includes only the Fe XVII lines and Fe XVI dielectronically formed satellites. The agreement is reasonably good, though both the 15.015 Å and 15.262 Å lines are slightly less intense than calculated.

This discrepancy cannot be attributed to optical thickness, the optical depth for the plasma being of order 10^{-4} or less, though possibly it is connected with the presence of the strong O VIII Ly- γ line at 15.18 Å (the O VIII Ly- β line at 16.01 Å is also present in this spectrum).

Since there is a negligible dependence of the theoretical line intensity ratio on N_e , we may transform the radial dependence

to one on T_e using Eq. (9). This is done in Fig. 12, in which a comparison is made with the theoretical dependence of this line intensity, illustrated in Fig. 4. As can be seen, the agreement between the two curves is close, though the increase of the $E(15.015\text{Å})/E(16.776\text{Å})$ with T_e is steeper for the theoretical curve than for the measured curve. This disagreement is probably associated with a number of uncertainties. First, the Abel inversion procedure is less accurate for radial distances smaller than that of the shell of maximum emission. Secondly, there are uncertainties in the functional form of the temperature (Eq. 9), in particular whether the exponent of the $(1 - r^2/a^2)$ term is really 2 or slightly more or less. Uncertainties in the central temperature (estimated to be 10%) also have an effect, as do the way in which the line intensity profiles as a function of chord distance are fitted (a fifth-order polynomial was used). Fig. 12 indicates with error bars the estimated uncertainties due to these effects. In view of the error bars, we regard the agreement of the two curves as confirmation of the theoretical intensities used in this work.

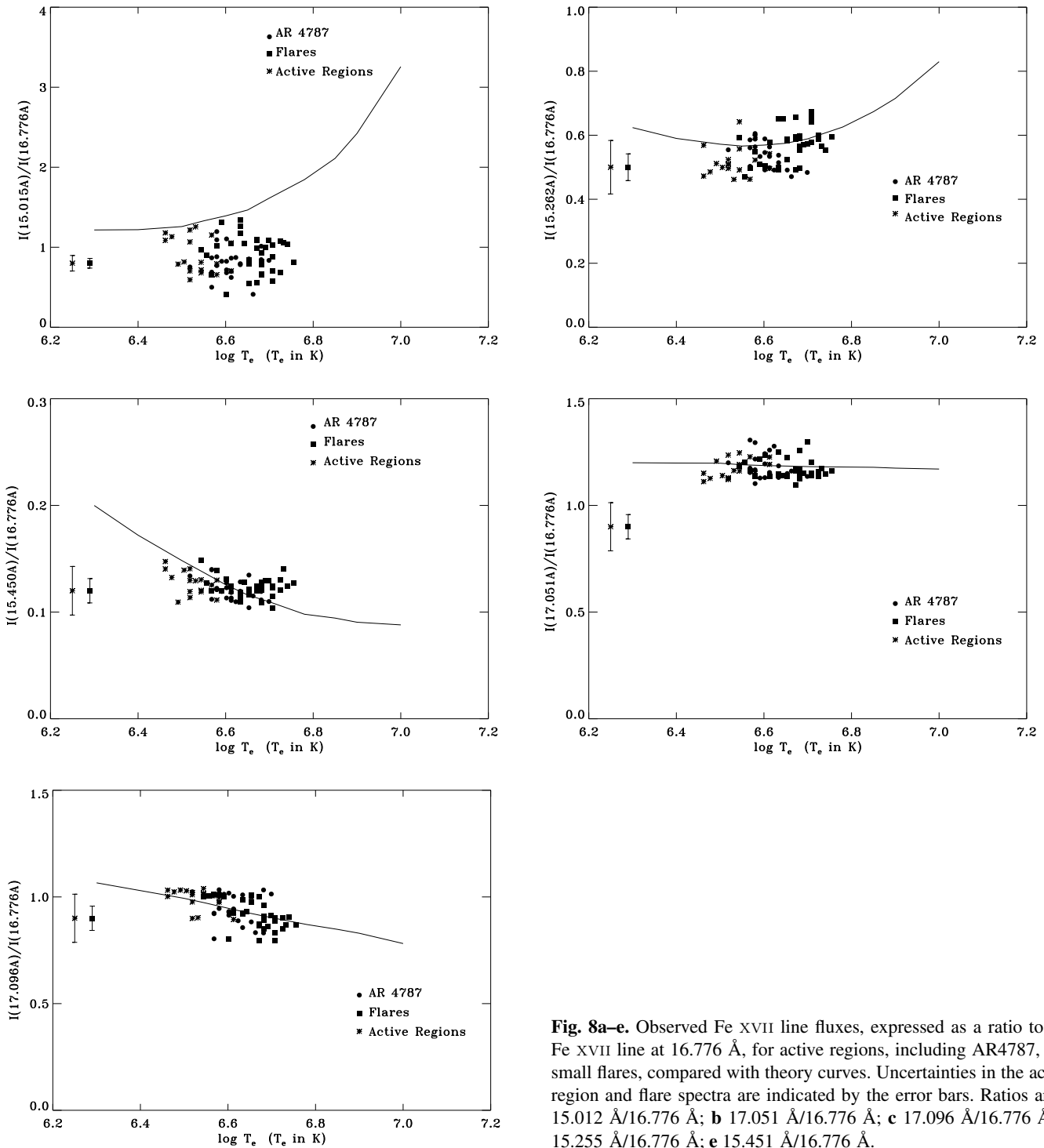


Fig. 8a–e. Observed Fe XVII line fluxes, expressed as a ratio to the Fe XVII line at 16.776 Å, for active regions, including AR4787, and small flares, compared with theory curves. Uncertainties in the active region and flare spectra are indicated by the error bars. Ratios are **a** 15.012 Å/16.776 Å; **b** 17.051 Å/16.776 Å; **c** 17.096 Å/16.776 Å; **d** 15.255 Å/16.776 Å; **e** 15.451 Å/16.776 Å.

A further confirmation of the accuracy of our synthetic spectra, and therefore the atomic data they are based on, is provided by a spectrum from the JET fusion device. It was obtained by a Bragg rotor spectrometer of similar design to the DITE instrument but with TIAP crystal ($2d = 25.76 \text{ \AA}$), giving central chord spectra. The radial position of maximum emissivity was found from an impurity transport code, SANCO-1D (Lauro-Taroni 1995). For the Fe XVII lines, this was found to be at

$r/a = 0.8$, where $N_e = 2.4 \times 10^{13} \text{ cm}^{-3}$ and $T_e = 6.45 \text{ MK}$ (560 eV). These values were used in calculating a synthetic spectrum, with which an observed spectrum (corrected for instrumental sensitivity) is compared in Fig. 13, as usual with the two spectra normalized to the 16.776 Å line. The agreement is very close for all Fe XVII lines, the 15.015 Å line being slightly more intense than expected. This slight disagreement is most likely due to the fact that the observed spectrum is a line-of-

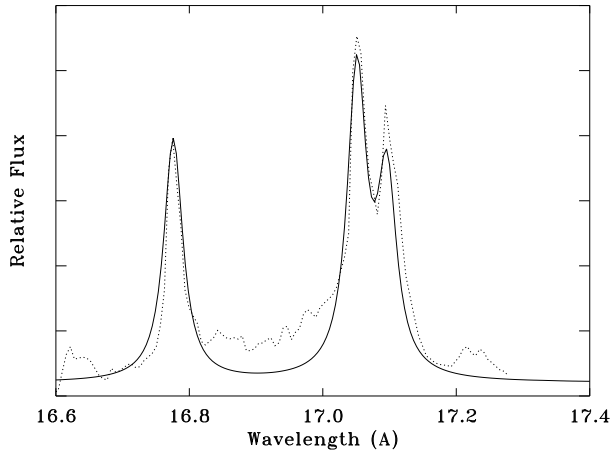


Fig. 9. Observed spectrum of Fe XVII lines in the 16.6–17.3 Å range from shot no. 24933 in the DITE tokamak, obtained with Johann spectrometer having curved KAP crystal and position-sensitive detector (dotted line), compared with synthetic spectrum (solid line) normalized to the Fe XVII 16.776 Å line, characterized by $T_e = 9$ MK and $N_e = 1 \times 10^{13} \text{ cm}^{-3}$.

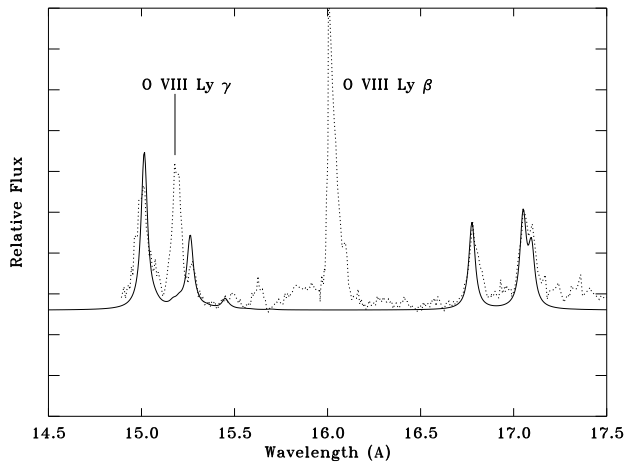


Fig. 10. Observed spectrum of Fe XVII lines in the 15–17 Å range from a central chord DITE plasma (shot no. 32507), taken with a Bragg rotor spectrometer (dotted line). It is compared with a theoretical Fe XVII spectrum (solid line) with $T_e = 6.5$ MK and $N_e = 3 \times 10^{13} \text{ cm}^{-3}$, i.e. parameters appropriate to the radial distance of maximum Fe XVII emissivity as deduced from Abel inversion techniques. The two spectra are normalized to the peak of the Fe XVII 16.776 Å line.

sight spectrum, involving regions of the emitting plasma that are both hotter and cooler than that of the maximum emissivity region. Note that, as with the DITE spectrum of Fig. 10, the presence of the O VIII lines creates some confusion in this region.

5. Summary

Our comparison of solar and tokamak Fe XVII X-ray spectra with synthetic spectra based largely on calculations of Fe XVII

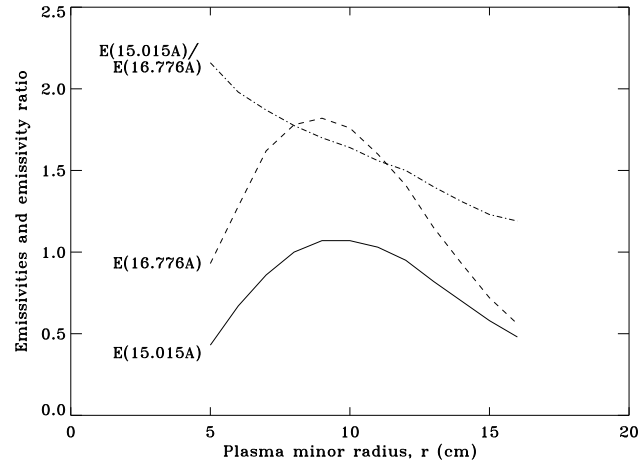


Fig. 11. Abel-inverted profiles of the Fe XVII lines at 15.015 Å and 16.776 Å in the DITE plasma, from observed spectra with various radial distances. The solutions are ill-behaved for radial distances $r < 5$ cm. The dot-dash curve shows the emissivity ratio of the 15.015 Å line to the 16.776 Å line.

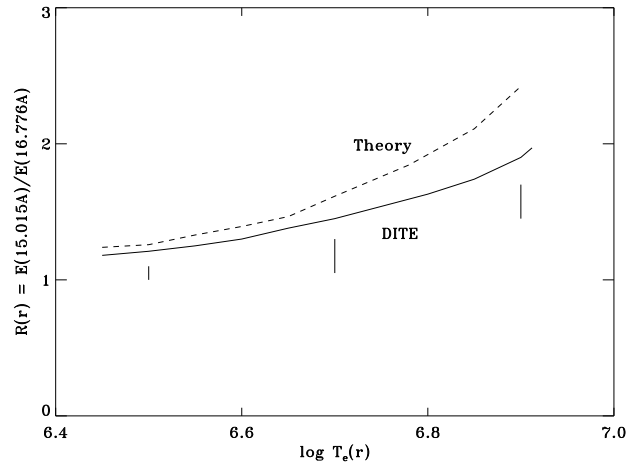


Fig. 12. The ratio of the Fe XVII line emissivity ratio, $E(15.015\text{Å})/E(16.776\text{Å})$ (solid line), as a function of T_e , derived from the profiles of Fig. 10, compared with the theoretical variation (dashed line). Short vertical lines represent uncertainties in the observed line ratio, due to the various causes mentioned in the text.

line intensities shows very good agreement. In the case of the solar spectra, the emitting plasma is insensitive to N_e but has slight sensitivity to T_e through the intensity ratio of the 15 Å and 17 Å lines. However, the resonance scattering of the 15.015 Å line which occurs for solar spectra means that this sensitivity cannot in practice be used as a temperature diagnostic. The Fe XVI dielectronic satellites which occur in this spectral region are T_e -sensitive, but they are weak, their theoretical wavelengths uncertain, and are blended with other lines; thus, they are not a reliable diagnostic of T_e . Instead, we derived T_e from the intensity ratio of the Fe XVII line at 16.776 Å to the Fe XVIII line at 16.073 Å; for the nearly isothermal active region spectra

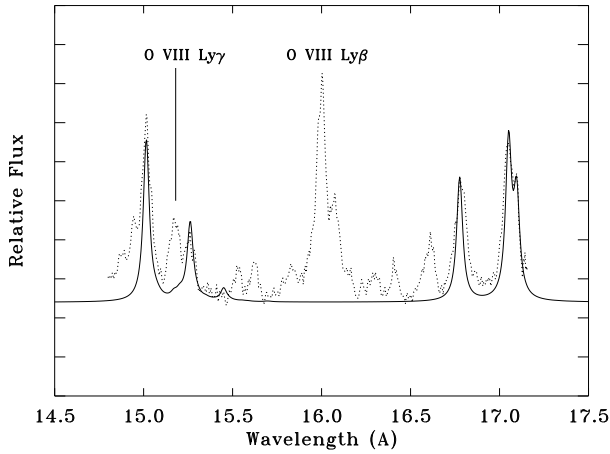


Fig. 13. Observed spectrum of Fe XVII lines in the 15–17 Å range from a JET plasma (shot no. 32797) with a Bragg rotor spectrometer (dotted line). It is compared with a theoretical Fe XVII spectrum (solid line) with $T_e = 6.5$ MK and $N_e = 3 \times 10^{13} \text{ cm}^{-3}$, i.e. parameters appropriate to the radial distance of maximum Fe XVII emissivity as deduced from the SANCO transport code. The two spectra are normalized to the peak of the Fe XVII 16.776 Å line.

T_e can be regarded as a true temperature but for flare spectra T_e is an average of the portion of the plasma emitting Fe XVII and Fe XVIII lines.

Both DITE and JET tokamak spectra agree well with theoretical spectra for temperatures and densities appropriate to the plasma shell having maximum emission. The density dependence of the Fe XVII $I(17.051 \text{ Å})/I(17.096 \text{ Å})$ ratio is confirmed for a DITE spectrum for which $N_e = 10^{13} \text{ cm}^{-3}$. Abel inversion techniques on a sequence of DITE spectra have enabled us to confirm the temperature dependence of the Fe XVII $I(15.015 \text{ Å})/I(16.776 \text{ Å})$ ratio. Thus, these tokamak spectra serve as useful ‘calibrators’, and confirm the reliability of the atomic data used in this analysis. We therefore have confidence that future analysis of Fe XVII X-ray spectra, such as those from astrophysical sources when they become available, could safely be based on the atomic data used here.

Acknowledgements. CJG and FPK acknowledge grants from the UK Royal Society and NATO (number CRG930722). The work of AKB was supported by NASA-RTOP grant 432-38-53-14. Dominic Zarro is thanked for providing analysis programs for the XRP data which have been extensively used in this work, and Michael Wilson and Robert C. Cowan for assistance with running the Cowan atomic code. We also thank Michael McSherry for programming help.

References

- Acton, L.W., et al. 1980, *Solar Phys.* 65, 53
- Allen, J.M., et al. 1986, *Plasma Phys. Controlled Fusion*, 28, 101
- Arnaud, M., Raymond, J.C. 1992, *ApJ* 398, 394 (ARA)
- Arnaud, M., Rothenflug, R. 1985, *A&AS* 60, 425
- Barnsley, R., Evans, K.D., Peacock, N.J., Hawkes, N.C. 1986, *Rev. Sci. Instrum.* 57(8), 2159
- Bely-Dubau, F., Dubau, J., Faucher, P., Gabriel, A.H. 1982, *MNRAS* 198, 239
- Bhatia, A.K. 1994, *At. Data Nucl. Data Tables* 57, 253
- Bhatia, A.K., Doschek, G.A. 1992, *At. Data Nucl. Data Tables* 52, 1
- Bhatia, A.K., Fawcett, B.C., Lemen, J.R., Mason, H.E., Phillips, K.J.H. 1989, *MNRAS* 240, 421
- Bhatia, A.K., Kastner, S.O. 1985, *Solar Phys.* 96, 11
- Brosius, J.W., Davila, J.M., Thomas, R.J., Monsignori-Fossi, B.C. 1996, *ApJS* 106, 143
- Burgess, A., Sheorey, V.B. 1974, *J. Phys. B* 7, 2403
- Cornille, M., Dubau, J., Faucher, P., Bely-Dubau, F., Blanchard, C. 1994, *A&AS* 105, 77
- Cornille, M., Dubau, J., Jacquemot, S. 1994, *At. Data Nucl. Data Tables* 58, 1
- Cornille, M., Dubau, J., Loulergue, M., Bely-Dubau, F., Faucher, P. 1992, *A&A* 259, 669
- Cowan, R.D. 1981, *The Theory of Atomic Structure and Spectra* (Berkeley: Univ. Colorado Press)
- Drayson, S.R. 1976, *J. Quantit. Spectrosc. Radiat. Transfer* 16, 611
- Duval, B.P., Bateman, J.E., Peacock, N.J. 1986, *Rev. Sci. Instrum.* 57(8), 2156
- Eissner, W., Seaton, M.J. 1972, *J. Phys. B* 5, 2187
- Eissner, W., Jones, M., Nussbaumer, H. 1974, *Comp. Phys.* 8, 270
- Erickson, G.W. 1977, *J. Phys. Chem. Ref. Data* 6, 831
- Feldman, U. 1993, *ApJ* 411, 896
- Feldman, U. 1995, *Comments in Atomic & Molecular Phys.* 31, 11
- Gabriel, A.H. 1972, *MNRAS* 160, 99
- Gabriel, A.H., Jordan, C. 1969, *MNRAS* 145, 241
- Harra-Murnion, L.K., et al. 1996, *A&A* 306, 670
- Jupén, C., Litzén, U. 1984, *Phys. Scripta* 30, 112
- Lauro-Taroni, L. 1995, *JET Laboratory Private Communication*
- Loulergue, M., Nussbaumer, H. 1975, *A&A* 45, 125
- McKenzie, D.L., Keenan, F.P., McCann, S.M. et al., 1992, *ApJ* 385, 378
- McKenzie, D.L., Broussard, R.M., Landecker, P.B. et al., 1980, *ApJ*, 238, L43
- Mohan, M. 1993, *Pramana* 40, 485
- Nilsen, J. 1989, *At. Data Nucl. Data Tables* 41, 131
- Phillips, K.J.H., et al. 1982, *ApJ* 256, 774
- Phillips, K.J.H., Harra, L.K., Keenan, F.P., Zarro, D.M., Wilson, M. 1993, *ApJ* 419, 426
- Phillips, K.J.H., Keenan, F.P., Harra, L.K. et al., 1994, *J. Phys. B* 27, 1939
- Phillips, K.J.H., Bhatia, A.K., Mason, H.E., Zarro, D.M. 1996a, *ApJ* 466, 549
- Phillips, K.J.H., Greer, C.J., Bhatia, A.K., Keenan, F.P. 1996b, *ApJL* 469, L57
- Raymond, J.C., Smith, B.W. 1986, *ApJ* 306, 762
- Rebut, P.H., et al. 1987, *Fusion Technology*, 11, 11
- Rugge, H.R., McKenzie, D.L. 1985, *ApJ* 297, 338
- Saba, J.L.R., Strong, K.T. 1992, *Proc. First SOHO Workshop*, Annapolis, Maryland, USA, ESA SP-348, 347
- Schmelz, J.T., Saba, J.L.R., Strong, K.T. 1992, *ApJ* 398, L115
- Smith, B.W., Raymond, J.C., Mann, J.B., Cowan, R.D. 1985, *ApJ* 298, 898
- Spitzer, L. 1962, *Physics of Fully Ionized Gases* (2nd ed.), Interscience Publishers, New York
- Waljeski, K., Moses, D., Dere, K.P. et al., 1994, *ApJ* 429, 909
- Warren, G.A., Keenan, F.P., Greer, C.J. et al., 1997, *Sol. Phys.* 171, 93